Journal of the Korean Ceramic Society
Vol. 50, No. 3, pp. 186~194, 2013.

http://dx.doi.org/10.4191/kcers.2013.50.3.186

Composition-property Relationships of Enamel Glass for Low Carbon Steel

Eun-Tae Kang†, Jong-Po Kim, Yong-Hyun Cho*, and Seon-Mi Park*

School of Nano & Advanced Materials Engineering, Engineering Research Institute, Gyeongsang University, Jinju 660-701, Korea

**Mold & Die Technology Team, Global Production Technology Center, Samsung Electronics Co., Ltd, Suwon 443-742, Korea*

(Received January 11, 2013; Revised May 10, 2013; Accepted May 28, 2013)

ABSTRACT

The relationship between composition and properties of enamel glass was investigated by introducing a mixture design. The enamel glass was manufactured by mixing various components under the following constraints: $45 \le SiO_2 \le 55$, $10 \le B_2O_3 \le 18$, $6 \le Na_2O \le 15$, $1 \le Li_2O \le 6$, $5 \le K_2O \le 10$, $0 \le TiO_2 \le 8$, $0 \le ZrO_2 \le 8$, 13.3MO (mol %). A mathematical model for the calculation of some properties of enamel glasses as a function of their composition was developed by the experimental statistical method. The results showed that the proposed model with the experimental measurement were in good agreement and the mixture experimental design was an effective method for optimizing the composition of the enamel glass with respect to its properties.

Key words : Enamel, Mixture design, Glass, Composition-Property relationship

1. Introduction

Porcelain enamel is generally defined as a substantially vitreous or glassy inorganic coating bonded to various metal substrates by fusion at a defined temperature.[1] Single-layer enameling has been increasingly used lately in the production of household equipment, architectural and construction parts, pipes, heat exchangers and is gradually displacing double-layer enameling that used to dominate. The new enameling method is not only an energy and resource saving technology due to decreasing the number of coat applications and firings but it also makes it possible to decrease the thickness of the coating because single-coat enameling prevents warping of large-size details. Accordingly, one-coat enamels have to meet certain requirements that have higher chemical strength, heat resistance, and adhesion strength and at the same time have good decorative and aesthetic properties.

The development of compositions for one-coat glass enamel with a decreased firing temperature is an important problem in enameling household steel products in view of decreasing the electricity cost. Glass enamel is typically alkali borosilicate where the alkalis are lithium, sodium, or potassium. Alkaline-earth ions such as calcium, strontium, or barium are also often present as fluxes. For adhesion, cobalt, nickel, iron, and copper are added to the glass. To develop compositions for one-coat glass enamel with a lower firing temperature the relationships between the components of the glass enamels and its properties must be known. However, it is difficult to understand the effect of each component on the properties of the glass enamel because of the complex composition.

Mixed designs are a mathematical method that obtains the mathematical relation between the constituent proportions and the responses. W with the help of mixed designs, we consider the relationships between the composition and its properties, taking into account requirements imposed on single-layer glass enamel with the help of mixed designs.

2. Experimental Procedure

Considering the reduction of the firing temperature, preliminary experiments and some reported studies[2-6], we limited the compositions of the glass enamel used in this work to a range as follows: $45 \le SiO_2 \le 55$, $10 \le B_2O_3 \le 18$, $6 \le Na_2O \le 15$, $1 \le Li_2O \le 6$, $5 \le K_2O \le 10$, $0 \le TiO_2 \le 8$, $0 \le ZrO_2 \le 8$, 13.3 MO (mol%). Here MO is the fixed complex oxide in mol% consisting of CaO (4.6), CaF_2 (3.45), CeO_2 (0.6), CoO (0.6), NiO (2.75), MnO_2 (0.6), Fe_2O_3 (0.3), CuO (0.4). The compositions selected as the mixed designs under these limits are shown in Table 1.

A batch of approximately 100 g was melted for 1-2 h at 1250°C in an alumina crucible placed in an electric furnace. The melt was then quenched between two cooled copper plates to create frit. Some melts were poured into a preheated graphite mold with a cylindrical shape and then annealed for 2 h at 10°C below the glass transition temperature.

The densities of the glass samples were measured using the Archimedes' principle with distilled water as the immersing fluid. The glass transition temperature (T_g), the softening temperature and the thermal expansion coefficient were measured using a dilatometer at a rate of 10°C/min. Young's modulus E and the shear modulus G were

†Corresponding author : Eun-Tae Kang
E-mail : etkang@gnu.ac.kr
Tel : +82-55-772-1681 Fax : +82-55-772-1689

Table 1. Compositions (mol%) Selected by DOE

No.	SiO_2	B_2O_3	Na_2O	Li_2O	K_2O	TiO_2	ZrO_2	MO*
1	48.7	13.2	9.5	2.8	7.2	3.2	2.1	13.3
2	55	10	6	2.7	5	8	0	13.3
3	55	10	15	1	5	0.7	0	13.3
4	45	18	6	5	5	4.2	3.5	13.3
5	48.1	12.6	15	1	10	0	0	13.3
6	45	10	15	1	7.9	8	0	13.3
7	46.7	10	6	1	10	8	5	13.3
8	45	18	15	1	5	2.7	0	13.3
9	55	11.59	6	1	5	3.7	4.5	13.3
10	55	18	6	2.7	5	0	0	13.3
11	45	17.3	12.4	5	7	0	0	13.3
12	48.9	13.8	6	5	8	0	5	13.3
13	45	10	11.7	5	10	0	0	13.3
14	55	10	6	5	10	0.7	0	13.3
15	48.7	13.2	9.5	2.8	7.2	3.2	2.1	13.3
16	47.7	18	6	5	10	0	0	13.3
17	45	10	6.8	5	6.9	8	5	13.3
18	45	13.4	9.3	1	5	8	5	13.3
19	55	10	6.7	5	5	0	5	13.3
20	55	10	6	1	10	0	4.7	13.3
21	45	12.7	6	5	10	8	0	13.3
22	46.9	18	6	1	6.8	8	0	13.3
23	45	18	6	1	10	1.7	5	13.3
24	48.7	13.2	9.5	2.8	7.2	3.2	2.1	13.3
25	49.02	18	8.68	1	5	0	5	13.3
26	45	11.7	15	5	5	0	5	13.3
27	45	10	15	5	5	6.7	0	13.3

*CaO 4.6, CaF_2 3.45, CeO_2 0.6, CoO 0.6, NiO 2.75, MnO_2 0.6, Fe_2O_3 0.3, CuO 0.4

obtained by the pulse-echo method with a Panametrics model 5800 pulser/receiver instrument with a quartz transducer. Both an X-cut transducer and a Y-cut transducer (with 10 MHz frequency) were employed for longitudinal modes and for shear modes, respectively. The pulse transient was measured with a Tektronix model TDS3012 oscilloscope. The method involves the transit-time measurement of short wave pulses traveling over a known path through the bulk of the specimen. The ratio of the path length to the transit time yields the velocity. From the sound velocity in longitudinal mode (V_L) and in shear mode (V_S) and the density (ρ) of the glass, the elastic parameters were calculated using the following equations.[7]

$$E=\frac{V_S^2(3V_L^2-4V_S^2)}{V_L^2-V_S^2} \qquad G=rV_S^2 \tag{1}$$

The Vickers hardness was determined using a Futuretech model FV-7E microhardness tester. The glass was indented by a Vickers diamond indenter at 1 kgf for 15 sec.

As a measure of chemical durability, the weight loss in 0.5N H_2SO_4 at 90°C was measured at a glass surface area to solution volume (SA/V) ratio of 0.01 cm^{-1}. The dissolution rate (DR) of bulk samples was calculated from the ratio of the fraction of weight loss $\Delta W/W$ versus the immersion time t. It was measured three times to obtain an average, and the error was estimated to be ±15%.

The wetting property on the low-carbon steel was expressed by contact angles and measured using a HK LAB model HKL-04-WASV high-temperature microscopy with a CCD camera. The contact angles were measured from the photographs of the samples maintained for 5 mins after raising temperature to 780°C at a rate of 20°C/min.

3. Results and Discussion

To design and analyze a mixture experiment, we have introduced pseudo-components, which are the linear transformation of the original components, because regression model fitting is much easier with the pseudo-component system than with the original component system when there are constraints on the components. We performed the statistical analysis of the data using the MINITAB,[8] which is a common statistical software. The function type of the angulation properties of enamels with the components was closely akin to the following polynomial

$$E(y)=\sum_{i=1}^{q}\beta_i x_i+\sum\sum_{i<j}\beta_{ij}x_i x_j \tag{2}$$

The statistical significance of the coefficients β_{ij} for each ingredient was confirmed by the t-test. The significance of the regression equation obtained from this was judged by the testing for lack of fit.

The regression model between the density and the composition for the investigated glasses has been estimated. First of all, we fitted a quadratic regression model based on the experimental data. The result of the t-test has shown that all the interaction effects are insignificant. The coefficients from the models in terms of the pseudo-components have been converted into those of the original components. The resulting fitted models are

$$\begin{aligned}&\rho(g/cm^3)\\&=1.657\times10^{-2}SiO_2+1.307\times10^{-2}B_2O_3+1.902\times10^{-2}Na_2O\\&+1.782\times10^{-2}Li_2O+1.575\times10^{-2}K_2O+2.885\times10^{-2}TiO_2\\&+4.295\times10^{-2}ZrO_2+9.073\times10^{-2}MO\end{aligned} \tag{3}$$

The statistical analysis of the predicted linear model for the density is shown in Table 2. The predicted values agree well with the experimental values. Fig. 1 shows a plot of the estimated densities from the model versus the corresponding measured values. It seems that the relation between two values is a straight line with slope 1 passing through the origin. That indicates that two values coincide nearly as 1 : 1. Thus the fitted model represents well the relationship

Table 2. Estimated Regression Coefficients for Density

Term	Coef.	SE Coef.	T	P	VIF
SiO_2	2.613	0.006008	*	*	1.638
B_2O_3	2.544	0.007498	*	*	1.857
Na_2O	2.661	0.006322	*	*	1.402
Li_2O	2.638	0.013336	*	*	1.936
K_2O	2.597	0.01129	*	*	1.758
TiO_2	2.856	0.006823	*	*	1.506
ZrO_2	3.135	0.010456	*	*	1.827
MO	4.081	0.605653	*	*	2.812
S = 0.006697343, R^2=99.35%, R_a^2=99.12%					

Coef: Least square estimator of regression coefficient,
T: Test statistic, P: p-value, VIF: variance inflation factor,
$S=\sqrt{MSE}$ (error mean of squares), R^2: coefficient of determination,
R_a^2: adjusted R^2

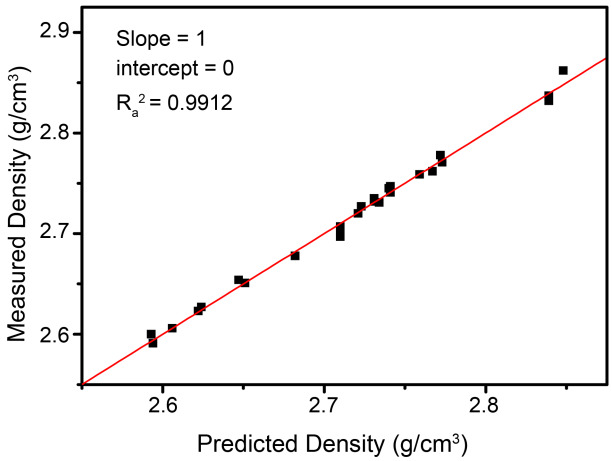

Fig. 1. Correlations between measured density and predicted density.

between the measured densities and the predicted values. The summary statistics for the above fitted models are R^2 = 99.35% and R_a^2 = 99.12%. R^2 represents the proportion of variation in the response densities that is explained by the model. It is known that the adjusted R^2 (R_a^2) is more appropriate than R^2 for comparing models with different numbers of predictors because it takes into consideration the number of predictors in the model. One very useful statistic for measuring the stability of a parameter estimate in a fitted model is the variance inflation factor (VIF) of the estimate. If any VIFs are greater than 10, then the corresponding least-squares estimates may be so poorly estimated that one should attempt to fit a different model form or use an alternative estimation procedure to that of least squares.[9] As Table 2 shows, the estimated coefficients of regression for the density were stable because the VIF values for the coefficients were lower than 3. The significance of the fitted model can be tested to determine which relationship is best between the response variable and the composition variables using the ANOVA. In the ANOVA the significance of the model terms is judged by the p-values. If the p-value is less than 0.05, the corresponding term is significant. As shown in Table 3 for all p-values, the probability of observing a value greater than or equal to F statistics in the F column of Table 3 is nearly 0. This indicates significant evidence of a linear regression model. The p-values for R^2, VIF and F test are the representing statistic whether the property values can be well explained by the components, but the reliability of the regression model cannot be evaluated. The reliability of the regression model is evaluated by the lack of fit test. The null hypothesis for a lack of fit test is that the equation used to describe how the independent variables relate to the dependent variables is correct. Because the p value for this case as shown in Table 3 is larger than the significant level of 0.05, the hypothesis that the model adequately fits the data must not be rejected. This indicates that the regression model on the density is adequate for the observed data at the significant level of 0.05.

Fig. 2 shows the response trace plot which describes the effect of incrementing the proportions of each component on the response. This figure was produced using the average of 27 compositions as the reference point. Each component shows a different effect on the density of enamel as shown in the Fig. 2. The effects of alkali oxides are essentially negligible. TiO_2 and ZrO_2, which have a big atomic weight, have a large effect on density.

The fitted model on the thermal expansion coefficient (α) is

Table 3. Analysis of Variance for Density

Source	DF	Seq SS	Adj SS	Adj MS	F	P
Regression	7	0.13089	0.13089	0.018699	417.36	0
Linear	7	0.13089	0.13089	0.018699	417.36	0
Residual error	19	0.000851	0.000851	0.000045		
Lack of Fit	17	0.000807	0.000807	0.000047	2.12	0.368
Pure error	2	0.000045	0.000045	0.000022		
Total	26	0.131741				

DF: Degrees of freedom, SS: Sum of squares
MS: Mean square, F: Test statistic, P: p-value

Table 4. Estimated Regression Coefficients for Some Properties

Properties	Interaction Term	T	P	VIF
CTE	$B_2O_3 \times Na_2O$	−3.07	0.008	2.673
	$B_2O_3 \times Li_2O$	−2.57	0.022	3.992
	$Na_2O \times K_2O$	−3.15	0.007	2.673
	$Li_2O \times TiO_2$	−2.35	0.033	3.805
	S=0.330927, R^2=97.51%, R_a^2=95.68%			
T_g	$SiO_2 \times K_2O$	2.65	0.018	3.265
	$SiO_2 \times TiO_2$	−4.84	0	2.616
	$Li_2O \times TiO_2$	2.68	0.017	3.908
	$TiO_2 \times ZrO_2$	4.18	0.001	3.826
	S=4.59307, R^2=98.80%, R_a^2=97.92%			
T_s	$Na_2O \times ZrO_2$	−3.13	0.006	2.793
	$TiO_2 \times ZrO_2$	2.52	0.022	3.705
	S=7.78179, R^2=96.05%, R_a^2=93.96%			
E	$SiO_2 \times B_2O_3$	2.79	0.016	3.053
	$SiO_2 \times Na_2O$	−5.19	0	3.215
	$SiO_2 \times ZrO_2$	−4.35	0.001	4.454
	$B_2O_3 \times Li_2O$	5.35	0	4.616
	$B_2O_3 \times TiO_2$	3.32	0.006	3.953
	$Na_2O \times Li_2O$	−3.8	0.003	4.284
	$Na_2O \times TiO_2$	−5.32	0	4.068
	S=1.15718, R^2=97.90%, R_a^2=95.44%			
G	$B_2O_3 \times Li_2O$	4.39	0	4.034
	$Na_2O \times ZrO_2$	7.05	0	2.894
	$Li_2O \times ZrO_2$	5.4	0	5.436
	S=0.529217, R^2=96.07%, R_a^2=93.61%			
H_v	$B_2O_3 \times Na_2O$	−5.32	0	3.338
	$B_2O_3 \times Li_2O$	−9.88	0	4.85
	$B_2O_3 \times TiO_2$	−9.41	0	3.513
	$B_2O_3 \times ZrO_2$	−18.5	0	5.206
	$Na_2O \times Li_2O$	−14.94	0	4.121
	$Li_2O \times TiO_2$	5.76	0	4.546
	$TiO_2 \times ZrO_2$	2.86	0.014	5.442
	S=3.12225, R^2=99.03%, R_a^2=97.90%			
DR	$SiO_2 \times B_2O_3$	−4.36	0.001	2.822
	$SiO_2 \times Na_2O$	−7.21	0	2.515
	$SiO_2 \times Li_2O$	−2.75	0.016	3.733
	$SiO_2 \times K_2O$	−6.58	0	3.841
	$Li_2O \times K_2O$	2.78	0.015	5.082
	S=0.97371, R^2=97.49%, R_a^2=95.35%			
Wetting Angle	$SiO_2 \times B_2O_3$	−3.63	0.003	2.896
	$SiO_2 \times Na_2O$	−8.37	0	2.745
	$SiO_2 \times Li_2O$	−10.24	0	4.521
	$SiO_2 \times ZrO_2$	3.42	0.005	4.208
	$Na_2O \times K_2O$	2.98	0.011	2.809
	$Li_2O \times TiO_2$	−5.47	0	4.862
	S=4.59307, R^2=98.80%, R_a^2=97.92%			

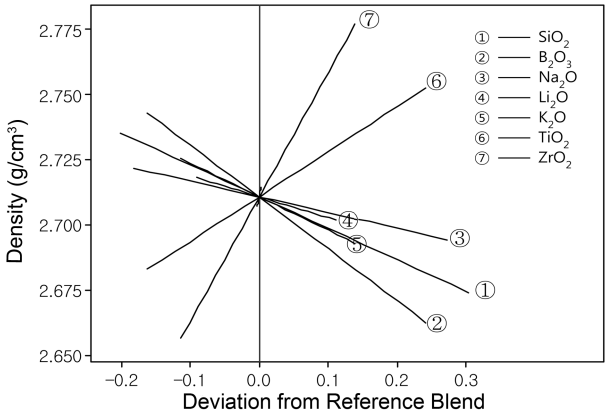

Fig. 2. Oxide component effects for model (3) fitted to data points.

$$\begin{aligned}\alpha(10^{-6}/^{o}\mathrm{C}) &= 1.031\times10^{-1}SiO_2+2.590\times10^{-1}B_2O_3+8.678\times10^{-1}Na_2O\\ &+7.996\times10^{-1}Li_2O+7.064\times10^{-1}K_2O+2.019\times10^{-1}TiO_2\\ &+3.163\times10^{-2}ZrO_2-5.780\times10^{-1}MO\\ &-1.73\times10^{-2}\cdot(B_2O_3\times Na_2O)-2.826\times10^{-2}\cdot(B_2O_3\times Li_2O)\\ &-2.763\times10^{-2}\cdot(Na_2O\times K_2O)-2.616\times10^{-2}\cdot(Li_2O\times TiO_2)\end{aligned} \quad (4)$$

The results of the t-test confirmed that only the interaction effects of ($B_2O_3 \times Na_2O$), ($B_2O_3 \times Li_2O$), ($Na_2O \times K_2O$), and ($Li_2O \times TiO_2$) are significant, as shown in Table 4. The summary statistics for the above fitted models are R^2 = 97.51% and R_a^2 = 95.68%. The p values and VIFs of the parameters for the each component on the thermal expansion coefficient are demonstrated to be statistically significance, although we did not include the estimated regression coefficients for the other properties due to the limited space α. Table 5 shows the ANOVA for the properties apart from density and the statistics for the lack of fit. It indicates that the quadratic regression model including the above interaction effects is also significant and that regression model (4) is adequate for the observed data at the significant level of 0.05. A plot of the estimated α versus the corresponding measured values reveals a straight line through the origin point with a slope of 1. The coefficient of determination R^2 was 0.9568. Fig. 3 shows the trace plot for α. The coefficient of thermal expansion decreases with an increasing SiO_2 and B_2O_3,which are network formers, and the effect of these components is the greatest of components. On the other hand, alkali increases the coefficient of thermal expansion and Li_2O has the weakest effect. Although TiO_2 and ZrO_2 reduce the coefficient of thermal expansion, these effects are modest.

The fitted model on the glass transition temperature (T_g) is

$$\begin{aligned}T_g(^{o}\mathrm{C}) &= 4.916SiO_2+6.455B_2O_3+0.12Na_2O-5.644Li_2O\\ &-12.889K_2O+22.821TiO_2+7.04ZrO_2+9.576MO\\ &+0.287\cdot(SiO_2\times K_2O)-0.384\cdot(SiO_2\times TiO_2)\\ &+0.419\cdot(LiO_2\times TiO_2)+0.506\cdot(TiO_2\times ZrO_2)\end{aligned} \quad (5)$$

Table 5. Analysis of Variance for Some Properties

Properties	Source	DF	SS	F	P
CTE	Regression	11	64.3373	53.41	0.000
	Linear	7	61.3067	57.25	0.000
	Quadratic	4	3.0306	6.92	0.002
	Residual	15	1.6427		
	Lack of fit	13	1.4090	0.93	0.631
	Pure error	2	0.2337		
	Total	26	65.9800		
T_g	Regression	11	26065.5	112.32	0.000
	Linear	7	24295.6	110.32	0.000
	Quadratic	4	1770.0	20.97	0.000
	Residual	15	316.4		
	Lack of fit	13	217.8	0.34	0.912
	Pure error	2	98.6		
	Total	26	26382.0		
T_s	Regression	9	25036.7	45.94	0.000
	Linear	7	23977.5	35.33	0.000
	Quadratic	2	1059.2	8.75	0.002
	Residual	17	1029.5		
	Lack of fit	15	977.0	2.48	0.325
	Pure error	2	52.5		
	Total	26	26066.2		
E	Regression	14	747.944	39.90	0.000
	Linear	7	620.960	66.99	0.000
	Quadratic	7	126.983	13.55	0.000
	Residual	12	16.069		
	Lack of fit	10	10.868	0.42	0.859
	Pure error	2	5.201		
	Total	26	764.012		
G	Regression	10	109.478	39.09	0.000
	Linear	7	86.340	35.17	0.000
	Quadratic	3	23.138	27.54	0.000
	Residual	16	4.481		
	Lack of fit	14	4.204	2.17	0.361
	Pure error	2	0.277		
	Total	26	113.959		
H_v	Regression	14	11959.6	87.63	0.000
	Linear	7	5105.0	103.29	0.000
	Quadratic	7	6854.6	100.45	0.000
	Residual	12	117.0		
	Lack of fit	10	105.2	1.79	0.411
	Pure error	2	11.7		
	Total	26	12076.6		
DR	Regression	12	516.782	43.07	0.000
	Linear	7	442.036	46.61	0.000
	Quadratic	5	74.746	14.95	0.000
	Residual	14	13.279	0.95	
	Lack of fit	12	12.571	1.05	0.28
	Pure error	2	0.708	0.35	
	Total	26	530.061		
Wetting angle	Regression	13	14249.2	38.67	0.000
	Linear	7	7413.0	14.99	0.000
	Quadratic	6	6836.2	40.20	0.000
	Residual	13	368.4		
	Lack of fit	11	362.9	12.01	0.079
	Pure error	2	5.5		
	Total	26	14617.6		

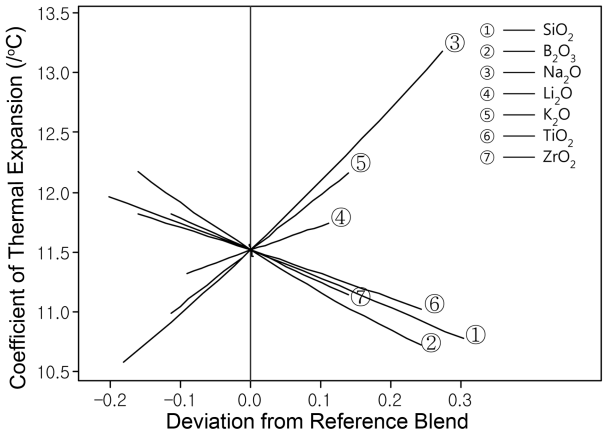

Fig. 3. Oxide component effects for model (4) fitted to data points.

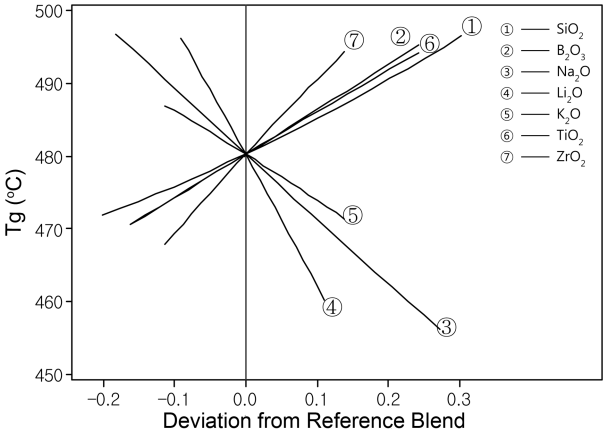

Fig. 4. Oxide component effects for model (2) fitted to data points.

The results of the *t*-test confirmed that the interaction of ($SiO_2 \times K_2O$), ($SiO_2 \times TiO_2$), ($Li_2O \times TiO_2$), and ($TiO_2 \times ZrO_2$), as shown in Table 4, are significant, which is unlike the case of the density and coefficient of thermal expansion. The statistics for the fitted models are R^2 = 98.80% and R_a^2 = 97.92%. The p values and VIFs of the parameters for each component is also statistically significant. Table 5 shows that regression model (5) is adequate for the observed data at a significant level of 0.05. Furthermore, a plot of the estimated T_g versus the corresponding measured values reveals a straight line through the origin point with a slope of 1. The coefficient of determination R^2 was 0.9792. Fig. 4 shows the trace plot for T_g. The glass former and TiO_2 and ZrO_2, which have high melting points, increases T_g but the alkali components clearly reduce T_g.

The fitted model on the glass softening temperature (T_s) is

$$\begin{aligned} T_s(^{\circ}\mathrm{C}) = {} & 2.346SiO_2 + 1.901B_2O_3 - 2.825Na_2O \\ & - 6.737Li_2O - 2.022K_2O + 1.608TiO_2 + 9.17ZrO_2 \\ & + 32.893MO - 0.688\cdot(Na_2O \times ZrO_2) \\ & + 0.508\cdot(TiO_2 \times ZrO_2) \end{aligned} \quad (6)$$

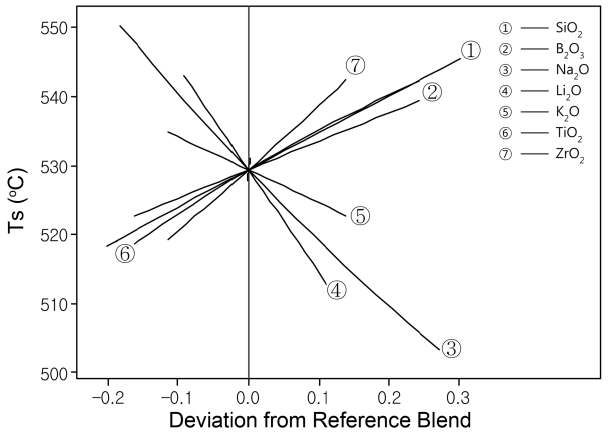

Fig. 5. Oxide component effects for model (6) fitted to data points.

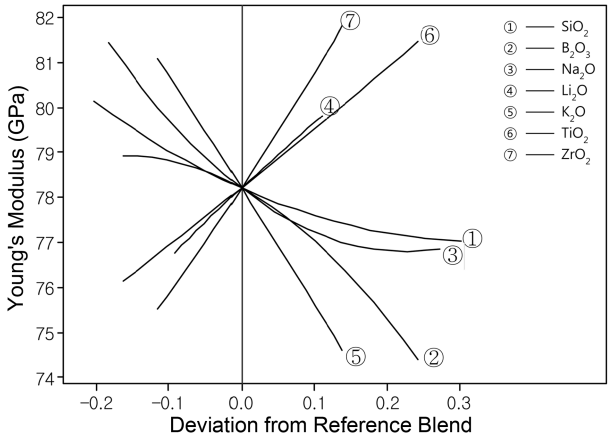

Fig. 6. Oxide component effects for model (7) fitted to data points.

The results of the *t*-test confirm that the interaction of only ($Na_2O \times ZrO_2$) and ($TiO_2 \times ZrO_2$), as shown in Table 4, is significant. The statistics for the fitted models are R^2 = 96.05% and R_a^2 = 93.96%. The *p* values and VIFs of the parameters for each component are also statistically significant. Table 5 confirms that regression model (6) is adequate for the observed data at the significant level of 0.05. Further, the plot of the estimated T_s versus the corresponding measured values reveals a straight line through the origin point with a slope of 1. The coefficient of determination R^2 was 0.9396. Fig. 5 shows the trace plot for T_s. The glass former and TiO_2 and ZrO_2, which have high melting points, increase T_s but the alkali components clearly reduce T_s as in the case of the glass transition temperature.

The fitted model on Young's modulus (*E*) is

$$\begin{aligned} E(GPa) = & -2.244SiO_2 - 6.642B_2O_3 + 3.14Na_2O - 3.305Li_2O \\ & - 3.634K_2O - 1.945TiO_2 + 4.502ZrO_2 + 22.516MO \\ & + 0.059 \cdot (SiO_2 \times B_2O_3) - 0.11 \cdot (SiO_2 \times Na_2O) \\ & - 0.12 \cdot (SiO_2 \times ZrO_2) + 0.221 \cdot (B_2O \times Li_2O) \\ & + 0.088 \times (B_2O \times TiO_2) - 0.146 \cdot (Na_2O \times Li_2O) \\ & - 0.12 \cdot (Na_2O \times TiO_2) \end{aligned} \quad (7)$$

There was the interaction of ($SiO_2 \times B_2O_3$), ($SiO_2 \times Na_2O$), ($SiO_2 \times ZrO_2$), ($B_2O_3 \times Li_2O$), ($B_2O_3 \times TiO_2$), ($Na_2O \times Li_2O$) and ($Na_2O \times TiO_2$) as shown in Table 4 according to the results of the *t*-test. The statistics for the fitted models are R^2 = 97.90% and R_a^2 = 95.94%. The *p* values and VIFs of the parameters for each component are also statistically significant. Table 5 shows that regression model (7) is adequate for the observed data at the significant level of 0.05. Further, the plot of the estimated *E* versus the corresponding measured values reveals a straight line through the origin point with a slope of 1. The coefficient of determination R^2 was 0.9544. Fig. 6 shows the trace plot for *E*. Unlike other properties, only TiO_2 and ZrO_2show positive effect.

The fitted model on the shear modulus (*G*) is

$$\begin{aligned} G(GPa) = & -3.289 \times 10^{-2} SiO_2 - 3.489 \times 10^{-1} B_2O_3 \\ & - 4.011 \times 10^{-1} Na_2O - 1.228 Li_2O - 4.025 \times 10^{-1} K_2O \\ & + 2.224 \times 10^{-1} TiO_2 - ZrO_2 + 3.318 MO \\ & + 7.771 \times 10^{-2} \cdot (B_2O_3 \times Li_2O) + 1.073 \\ & \times 10^{-1} \cdot (Na_2O \times ZrO_2) + 1.407 \times 10^{-1} \cdot (Li_2O \times ZrO_2) \end{aligned} \quad (8)$$

The results of the *t*-test displayed the interaction of ($B_2O_3 \times Li_2O$), ($Na_2O \times ZrO_2$), and ($Li_2O \times ZrO_2$) as shown in Table 4. The statistics for the fitted models are R^2 = 96.07% and R_a^2 = 93.61%. The *p* values and VIFs of the parameters for each component are also statistically significant. Table 5 confirms that regression model (8) is adequate for the observed data at a significant level of 0.05. A plot of the estimated *G* versus the corresponding measured values reveals a straight line through the origin point with a slope of 1. The coefficient of determination R^2 was 0.9361. Fig. 7 shows the trace plot for *G*. Only TiO_2 and ZrO_2 show a positive effect like Young's modulus.

The fitted model on the hardness (H_V) is

$$\begin{aligned} H_V = & 6.664SiO_2 + 20.409B_2O_3 + 12.857Na_2O + 31.126Li_2O \\ & + 3.29K_2O + 12.526TiO_2 + 33.432ZrO_2 - 17.57MO \\ & - 0.316 \cdot (B_2O_3 \times Na_2O) - 1.131 \cdot (B_2O_3 \times Li_2O) \\ & - 0.637 \cdot (B_2O_3 \times TiO_2) - 1.877 \cdot (B_2O_3 \times ZrO_2) \\ & - 1.515 \cdot (Na_2O \times Li_2O) + 0.661 \cdot (Li_2O \times TiO_2) \\ & + 0.28 \cdot (TiO_2 \times ZrO_2) \end{aligned} \quad (9)$$

Table 4 shows the interaction of ($B_2O_3 \times Na_2O$), ($B_2O_3 \times Li_2O$), ($B_2O_3 \times TiO_2$), ($B_2O_3 \times ZrO_2$), ($Na_2O \times Li_2O$), ($Li_2O \times TiO_2$), and ($TiO_2 \times ZrO_2$) according to the results of the *t*-test. The statistics for the fitted models are R^2 = 99.03% and R_a^2 = 97.90%. The *p* values and VIFs of the parameters for each component are also statistically significant. Table 5 confirms that the regression model (9) is adequate for the observed data at a significant level of 0.05. A plot of the esti-

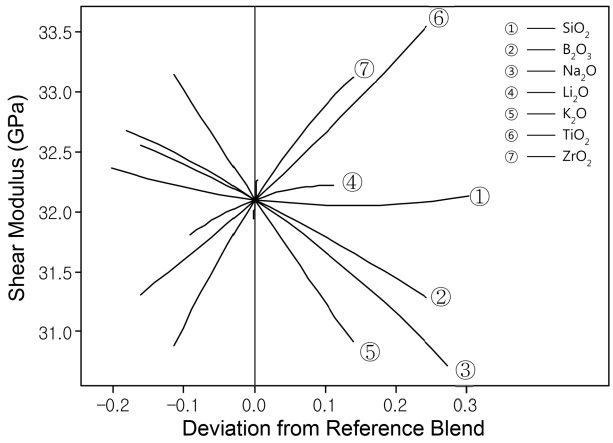

Fig. 7. Oxide component effects for model (8) fitted to data points.

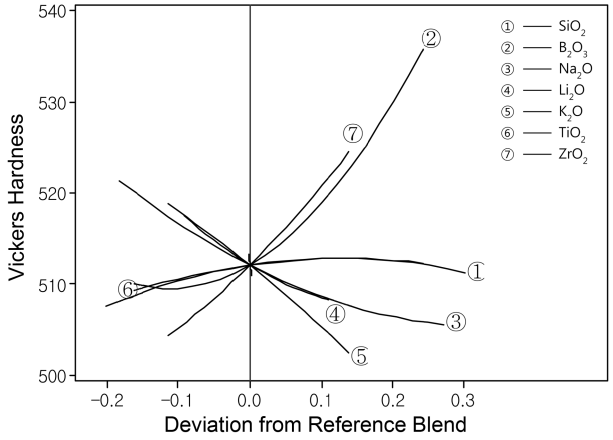

Fig. 8. Oxide component effects for model (9) fitted to data points.

mated H_V versus the corresponding measured values shows a straight line through the origin point with a slope of 1. The coefficient of determination R^2 was 0.9790. Fig. 8 shows the trace plot for H_V. Alkali components had a negative effect but B_2O_3 and ZrO_2 had a strong and positive effect on the enhancement of hardness.

The fitted model on the chemical durability (*DR*) is

$$\begin{aligned} &DR(10^{-2}/\text{min}) = \\ &0.861SiO_2+1.904B_2O_3+4.242Na_2O \\ &+1.299Li_2O+6.536K_2O-0.249TiO_2-2.121ZrO_2 \\ &+1.756MO-0.075\cdot(SiO_2\times B_2O_3)-0.114\cdot(SiO_2\times Na_2O) \\ &-0.079\cdot(SiO_2\times Li_2O)-0.164\cdot(SiO_2\times K_2O) \\ &+0.139\cdot(Li_2O\times K_2O) \end{aligned} \quad (10)$$

Table 4 shows the interaction of ($SiO_2 \times B_2O_3$), ($SiO_2 \times Na_2O$), ($SiO_2 \times Li_2O$), ($SiO_2 \times K_2O$), and ($Li_2O \times K_2O$) according to the results of the *t*-test. The statistics for the fitted models are $R^2 = 97.49\%$ and $R_a^2 = 95.35\%$. The *p* values and VIFs of the parameters for each component are also statistically significant. Table 5 confirms that regression model (10) is adequate for the observed data at a significant level of 0.05. A plot of the estimated *DR* versus the corresponding measured values reveals a straight line through the origin point with a slope of 1. The coefficient of determination R^2 was 0.9535. Fig. 9 shows the trace plot for the *DR*. It is shown that the alkalis are the ingredients components that lowers more resistance to acid. SiO_2, TiO_2, and ZrO_2 effectively improve the chemical durability but B_2O_3 is unable to improve the chemical durability which was different from our expectations. This indicates the possibility of the phase separation of these enamels with an interconnected structure.

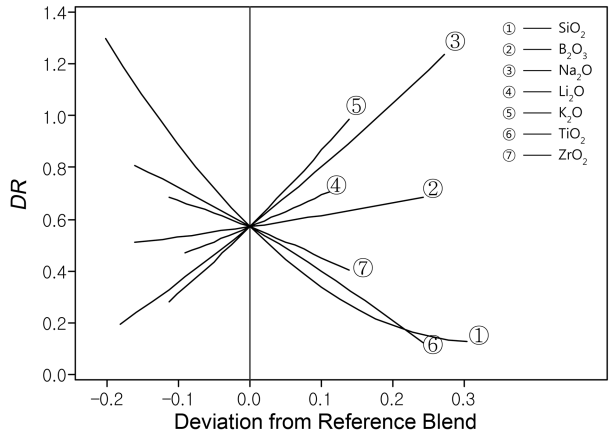

Fig. 9. Oxide component effects for model (10) fitted to data points.

The wetting behavior of the solid-liquid interface can be understood from the wetting angle. The fitted model of the wetting angle is

$$\begin{aligned} &Wetting\ angle(^o) = \\ &-3.446SiO_2-2.460B_2O_3+18.110Na_2O+65.596Li_2O \\ &-18.043K_2O-13.664TiO_2-35.572ZrO_2+67.163MO \\ &-0.345\cdot(SiO_2\times B_2O_3)-0.754\cdot(SiO_2\times Na_2O) \\ &-1.774\cdot(SiO_2\times Li_2O)+0.423\cdot(SiO_2\times ZrO_2) \\ &+0.430\cdot(Na_2O\times K_2O)-1.106\cdot(Li_2O\times TiO_2) \end{aligned} \quad (11)$$

Table 4 shows the interaction of ($SiO_2 \times B_2O_3$), ($SiO_2 \times Na_2O$), ($SiO_2 \times Li_2O$), ($SiO_2 \times ZrO_2$), ($Na_2O \times K_2O$) and ($Li_2O \times TiO_2$) according to the results of the *t*-test. The statistics for the fitted models are $R^2 = 97.48\%$ and $R_a^2 = 94.96\%$. The *p* values and VIFs of the parameters for each component are also statistically significant. Table 5 confirms that regression model (11) is adequate for the observed data at a significant level of 0.05. A plot of the estimated wetting angle versus the corresponding measured values reveals a straight line through the origin point with a slope of 1. The coefficient of determination R^2 was 0.9496. Fig. 10 shows the trace plot for the wetting angle. Na_2O and K_2O among alkali components increase the wetting angle, while by contrast Li_2O reduces it. TiO_2 and ZrO_2 also have an increasing wetting angle. On the other hand, SiO_2 and B_2O_3 reduce the wetting angle but B_2O_3 is lower than SiO_2.

Table 6. Optimization Design Criterion and Optimal Solutions, and Comparison of the Properties Obtained from Experimental and Predicted Models

	Optimized 1			Optimized 2		
	Lower	Target	Higher	Lower	Target	Higher
CTE	10.5	11	11.5	10.5	11	11.5
T_g		Minimized			Minimized	
T_s		Minimized			Minimized	
HV		Maximized			Maximized	
DR		Minimized			Minimized	
Wetting angle		-			Minimized	

	SiO_2	B_2O_3	Na_2O	Li_2O	K_2O	TiO_2	ZrO_2	MO
Optimized 1	48.08	17.99	9.21	4.41	5.16	1.87	0	13.3
Optimized 2	50.79	17.06	7.56	3.88	7.17	0	0.24	13.3

		ρ (g/cm^3)	α (10^{-6}/°C)	T_g (°C)	T_s (°C)	E (GPa)	G (GPa)	H_V	DR (10^{-2}/min)	$W.A$ (°)
Optimized 1	Predicted	2.627	10.83	472	521	81	32	530	4	24
	Measured	2.632	11.05	471	520	80.8	31.6	528	2.5	25.7
Optimized 2	Predicted	2.607	11.1	480	528	78	31	535	3	20.6
	Measured	2.609	10.88	481	523	78.8	30.8	537	2.2	21.4

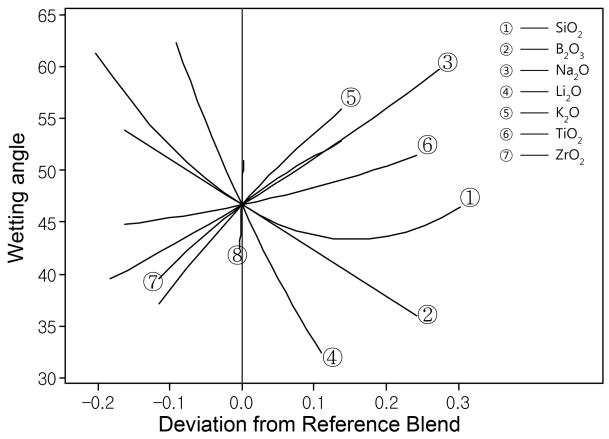

Fig. 10. Oxide component effects for model (11) fitted to data points.

The D-optimality criterion,[10] which minimizes the variance in the regression coefficients of the fitted model, has been used to identify the composition that offers the optimum enamel glass for low-carbon steel. Table 6 defines the design optimization parameters and lists the optimal compositional solutions based on the data obtained and models utilized in this work. To examine the precision of the model and the accuracy of the results, two optimized formulations as shown in Table 6 were selected and the result of the experiment and the model's predicted values have been compared. The difference between the two optimized formulations is whether it contains a wetting angle as a variable for optimization of the composition. The results show that the experimental and predicted values of all properties are in good agreement with acceptable accuracy whether or not the contact angle variable is considered. There is no clear difference in physical properties between the two optimized compositions. That means that the optimized composition is robust against some degree of change in the composition. However, if the chemical durability and wetting angle are more important than others, the optimized 2 composition is more desirable.

4. Conclusions

The relationships between the components and properties of enamel glasses for low-carbon steel were obtained on the basis of a mixture design experiment with multicomponent constraints. These relationships on various properties were statistically significant. On the basis of these relations we analyzed the effect of each component and of the interaction between the components on the properties. The preferred compositions for one-coat glass enamel with a low firing temperature, derived from the desirability analysis by weighing the chemical durability and wetting angle, is as follows (mol%): 50.79 SiO_2, 17.06 B_2O_3, 7.56 Na_2O, 3.88 Li_2O, 7.17 K_2O, 0.24 ZrO_2, 13.3 MO.

REFERENCES

1. J. C. Oliver, "Porcelain Enamels-Review and Outlook," *Am. Ceram. Soc. Bull.*, **62** [5] 562-63 (1983).
2. H. Murakami and S. Nishimura, "Product for Enameling and Enameled Product," U.S. Pat. No: A1 0040872 (Feb. 18, 2010).
3. L. L. Bragina and G. K. Voronov, "Effect of a Complex of Aliovalent Cations on Processes in an Enamel Melt-Low Carbon Steel System," *Glass Ceram.*, **65** 59-62 (2008).

4. E. A. Yatsenko, "Specific Features of the Resource-Saving Technology of Functional Single-Layer Composite Enamel Coatings for Steel," *Glass Phys. Chem*., **37** [1] 41-50 (2011).
5. Mobay Co., "Enamel Compositions," E.P. Pat. No:A1 0446477 (Dec. 21, 1990).
6. H. J. Schttenhelm and W. Joseph, "Enamel Frits for Sheet Steel with Improved Bonding," U.S. Pat. No: 4847218 (Jul. 11, 1989).
7. H. J. McSkimin "Note and References for the Measurement of Elastic Moduli by Means of Ultrasonic Waves," *J. Acous. Soc*., **33** [5] 606-16 (1961)
8. MINITAB Release 14.20, Minitab Inc. (2005).
9. D. W. Marquardt, "Generalized Inverses, Ridge Regression, Biased Linear Estimation and Nonlinear Estimation," *Technometrics*, **12** [3] 591-612 (1970).
10. J. A. Cornell, "Experiments with Mixtures, Designs, Models, and the Analysis of Mixture Data," 3rd Ed., pp. 400-01, Wiley, New York, 2002.